Structural, optical, and resistive switching behavior in SnO$_2$ and Schiff-based SnO$_2$ nanoparticles

Monika Duhan[1], Manpreet Kaur[1], Sanjeev Kumar[2], Gyaneshwar Sharma[3,*] ⓘ, and Harminder Kaur[1,*]

[1] *Chemistry Department, Punjab Engineering College (Deemed to Be University), Chandigarh 160012, India*

[2] *Physics Department, Punjab Engineering College (Deemed to Be University), Chandigarh 160012, India*

[3] *Department of Physics, Tilak Dhari P.G. College, Jaunpur, Uttar Pradesh 222002, India*

ABSTRACT

Phenomenon of resistive switching and alteration of resistive state under the gradient of electrical potential is observed in metal oxides thin film. Such type of activity is exploited in Resistive switching-based memory devices. Here, we report electric field-induced switching behavior from one resistive state to other resistive state in nano-sized SnO$_2$ and Schiff base-modified SnO$_2$ materials. From the gradually rise in interest toward more reliable and high energy storage devices, metal oxides with Schiff base doping are investigated. Instability in resistive state of metal oxides are driven through field-induced lattice distribution which causes a scattering of mobile electron of different strength. The emergence of resistive switching in SnO$_2$ along with Ohmic nature. Resistive switching behavior is less studied in bulk form; but such unconventional type of approach provides a more space toward the theoretical studies and their proper understanding.

1 Introduction

The past few decades have been witnessed significant advances in the field of memory storage via elucidation of state-of-art device miniaturization technique, theoretically demanded novel compositions of smart materials, and followed by proper assessment of governing mechanism. Various types of materials have been investigated for memory storage processing. Initially, materials demonstrate ferroelectric ordering, magnetic ordering, modulation in resistivity with exposure to magnetic field, semiconductor due to switching property of certain physical property (polarization, magnetization, resistivity). On the basis of above physical response, a range random access memory (RAM) devices have been realized, for example, Ferroelectric RAM (FeRAM), Magnetoelectric RAM (MeRAM), Magnetoresistance RAM (MRAM), Tunnel Magnetoresistance (TM), and Phase Change RAM (PRAM). Till now, MRAM are available for commercial purpose. In this device, data is written by switching the magnetic states ($\pm$ M) upon application of a magnetic field while to read data, one exploits variation of magnetoresistance in the magnetic states. Being hard ferromagnets, the materials in the MRAMs possess high coercivity resulting in large magnetic field requirement for switching magnetic states and thus consume large amount of energy and this limits the performance of magnetism-based devices. In contrast, ferroelectric memories (FeRAMs) possess faster writing speeds via achieving bi-stable polarization state and are energy efficient. FeRAMs devices are still under progress,

---

Springer

desired storage density of gigabyte level has not been achieved yet. Moreover, most efficient ferroelectric materials ($PbZr_xTi_{1-x}O_3$, $SrBi_2Ta_2O_9$) are being used for RAM purpose only, magnitude of polarization in these materials is large but there is no further scope toward improvement in degree of polarization. The limitation on polarization magnitude leads no room for further scope of progress in FeRAM technology.

To realize a memory device (*small, cheap, fast, and reliable*), various techniques are being seriously pursued. In principle, MRAM and PRAM are similar to RRAM. From mechanism point of view; MRAM, PRAM, and RRAM are qualitatively different from each other. First two approaches have been well explored from mechanism viewpoint while RRAM is relatively less understood. Due to its promising characteristics and ranked efficiency, RRAM are being extensively explored without paying much attention on their governing mechanism [1–5]. However, these have limitations on their size and show slow readability due to their destructive read operation and subsequent reset. With these unfavorable circumstances, present technology has grown at satisfactory level but—with ever-increasing prolific demand and affinity toward "ultimate memory devices"- various important parameters – governing important role in function of memory devices are yet to be addressed. In order to meet switching-based devices with ultimate performance (non-volatile, dense, robust, fast, good endurance and retention property, less energy expensive, high ON–OFF ratio), the researcher from academic and industrial institution are having attention toward other physically equivalent approach to realize a switching device with improved performance. Apart from having great contribution in memory storage, these switching devices have been promisingly mimics as synapses for neuromorphic activity.

SnO_2 is a widely used material in gas-sensing technology, owing to its desirable physical–chemical properties and benefits from its porous structure. However, from a gas-sensing application perspective, SnO_2 suffers from high operating temperatures, low sensitivity, and poor selectivity. Recent advancements in synthesis and characterization have enabled SnO_2 nanomaterials to exhibit improved gas-sensing performances. SnO_2 materials with diverse morphologies and texturing have achieved enhanced sensing performances. Furthermore, recent studies have demonstrated that SnO_2 is capable of exhibiting threshold-switching phenomena, characterized by a rapid transition from

a high resistance state to a low resistance state upon reaching a specific threshold voltage. This property holds significant potential for utilization in high-speed electronic devices. Akbari-Saatlu et al. have remarkably demonstrated the good sensing sensitivity of SnO2 toward minute exposures of CH_3SH and H_2S gases across a broad concentration range. Koliopoulou et al. reported on the realization of a low-temperature processed, Electrically Erasable Programmable Read-Only Memory (EEPROM)-like device. The electrical characteristics of the final hybrid Metal–Insulator-Semiconductor (MIS) memory cells were evaluated in terms of memory window and program/erase voltage pulses [6–8].

Metal oxides are well known having resistive switching phenomenon. Various binary metal oxides TiO_2 [9], NiO [10], Nb_2O_5, ZrO_2, MgO, CoO, HfO_2 [11], ZnO [12], SnO_2, CuO, Ga_2O_3, AlO_x [13], graphene oxides have been studied [14]. SnO2 has a wide bandgap and n-type semiconducting characteristics. Hafnium oxide (HfO_x) is a strong candidate for resistive switching memories due to its excellent performance with the higher endurance, ultra-high switching speed, data reliability, and multilevel storage capability. ZnO is another n-type semiconductor, exhibits low toxicity and high stability in their switching behavior. Perovskite materials like $(Ba,Sr)TiO_3$ [15], $SrZrO_3$, $BiFeO_3$, and $(Pr,Ca)MnO_3$ [16] have also been studied. Dielectric materials with large band gap like Al_2O_3 and Gd_2O_3 and chalcogenides (In_2Se_3 and In_2Te_3) are promising candidates in this area [1]. There are large group of materials which belongs to resistive switching family, but the mechanism of switching is not clear yet.

SnO_2 is optically transparent n-type semiconductor material with band gap of 3.6 eV. Though tin oxide is considered as important candidate in the field of technology for exhibiting excellent optical, gas-sensing for extremely stable in harsh condition and transparent conducting electrode, it has gained attention in resistive switching memory [17]. Here, we observe resistive switching in Schiff base SnO_2 material with two probe electrical resistivity measurement configuration rather than parallel capacitive form. Schiff bases contain the azomethine group (–RC = N–) and are usually formed by the condensation of a primary amine with an active carbonyl compound [18, 19]. Further, Schiff base compounds are found to be very promising because of their biodegradability, non-toxicity, good electrical conductivity in conjugated compounds, cheaper, and easy production. They are stable and can tune the

ligational aspects by varying denticity and basicity. Due to these interesting properties of Schiff bases, I-V characteristics of Schiff-based SnO_2 were found to be enhanced. Probably, this study will provide relaxation to the manufacturer of switching devices and their theoretical modeling toward the scalability, stability, switching speed and mechanism.

2 Experimental details

Schiff base was synthesized by simple conventional method of refluxing using o-vanillin (0.456 g, 3 mmol) and p-toluidine (0.321 g, 3 mmol). A clear solution was obtained by dissolving starting materials in minimum amount of ethanol- water mixture (2:1, 15 ml). The obtained reaction mixture was then refluxed with constant stirring for 3 h. Dark orange colored crystalline product was obtained by filtration after 24 h.
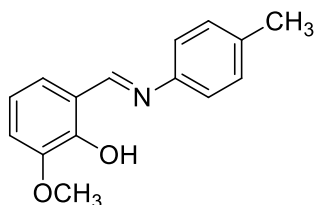
(*E*)-2-methoxy-6-((*p*-tolylimino)methyl)phenol

Schiff Base-doped tin oxide nanoparticles were prepared by sol–gel method. Appropriate amount of Schiff base was dissolved in tin tetrachloride pentahydrate ($SnCl_4 \cdot 5H_2O$) in ethylene glycol. Resultant mixture was then stirred for three hours till the solution becomes transparent. The reaction mixture was heated up with stirring at 120 ℃ till it reduces to one third of its original volume. The gel formed was calcined at 600 ℃ for two hours at the rate of 2 ℃ min^{-1}. The obtained powder is dried in pestle and mortar.

For the I-V characteristics measurement, two electrical terminals contacts were developed with silver paste and connected to the Source meter and Nanovoltmeter (Kiethley Instrument Inc.). I-V data was collected with LabVIEW program. At room temperature, the crystallite size and phase purity of synthesized samples were determined by using X-ray Diffraction (XPERT-PRO). Observed X-ray diffraction patterns were refined with GSAS-EXPGUI software. Transmission Electron Microscopy of JEOL (JEM-1011) was used to study the TEM images of all the prepared samples. The presence of surface defects like oxygen and tin vacancies were studied by Photoluminescence Spectroscopy (RF-5301). To understand the functional groups present in the system, Fourier Transform-Infrared (FT-IR) spectra were recorded using Perkin Elmer Spectrum two. Magnetic measurements of pure SnO_2 and Schiff base-doped SnO_2 were recorded by using Vibrating Sample Magnetometer (Microsense EZ 9).

3 Results and discussion

Figure 1 shows the X-ray diffraction patterns of pure SnO_2 (A1) and Schiff base-doped SnO_2 (A2) nanoparticles. Phase purity and tetragonal symmetry (space group P4$_2$/mnm) of synthesized samples were investigated through the analysis of X-ray diffraction (XRD) patterns. Rietveld refinement of XRD patterns of A1 and A2 were performed by using GSAS – EXPGUI software. No additional peaks were observed in XRD

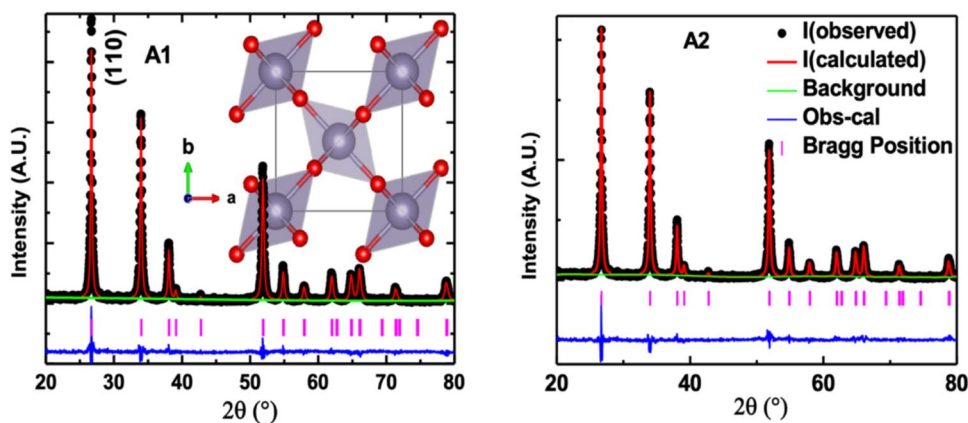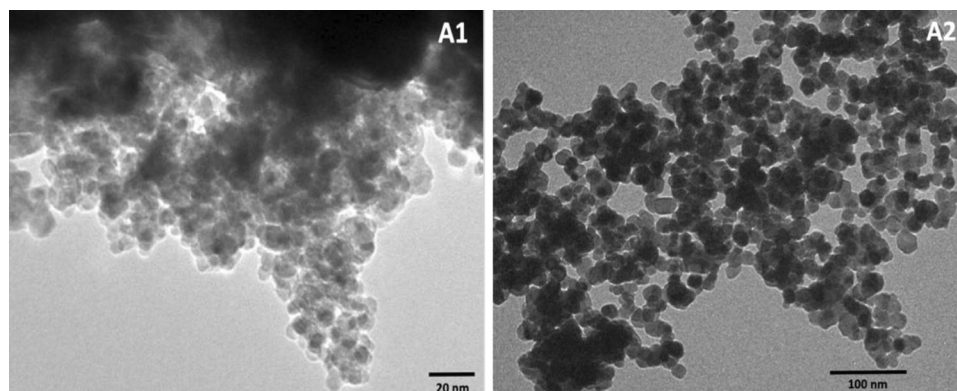**Fig. 1** XRD patterns of (A1) pure SnO_2 and (A2) Schiff base-doped SnO_2

Fig. 2 TEM micrographs of (A1) pure SnO_2 and (A2) Schiff base-doped SnO_2

pattern which suggests that synthesized systems have no any unreacted ingredients. Cell parameters for A1 sample were found to be a = 4.742 (2) Å, b = 4.742 (2) Å, c = 3.189(1) Å, V=71.724 Å^3 and Wyckoff position Sn (0.000, 0.000, 0.000) and O (0.307, 0.307, 0.307) and A2 exhibits unit cell parameter 4.741 (2) Å, 4.741(2) Å, 3.189(1) Å, and V=71.724 Å^3. The crystallite size was found to increase from 12 to 31 nm with the incorporation of Schiff base in tin oxide lattice, estimated from Debye – Scherer equation [20]. The observed intensity of Bragg reflection peak (110), centered at 26.6° is higher than the calculated intensity which suggests that microstructures of SnO_2 have grown preferably along (110) plane [21, 22]. Figure 2 shows TEM micrograph of both samples A1 and A2. Particle size distribution analysis is consistent with results obtained from XRD. It is observed that microstructure of A1 grows with irregular geometry (average particle size ~ 13 nm) and A2 are found to be spherical nature and comparatively larger in size (average particle size ~ 22 nm). It also reveals that Schiff base doping causes considerable change in shape, size, and narrow crystallite distribution of microstructures of synthesized samples.

To understand the presence of different functional groups in the lattice, FTIR spectra of pure and Schiff base-doped tin oxide nanoparticles has been recorded and shown in Fig. 3. The main hump around 3400 cm^{-1} in the spectra is attributed to the O–H stretching vibration. Bending vibrations at 1624 cm^{-1} corresponds to the water content adsorbed on the surface of samples. In the crystalline phase, the presence of SnO_2 was confirmed by the peak observed at 616 cm^{-1} which is due to the O–Sn–O stretching vibration in the system [23].

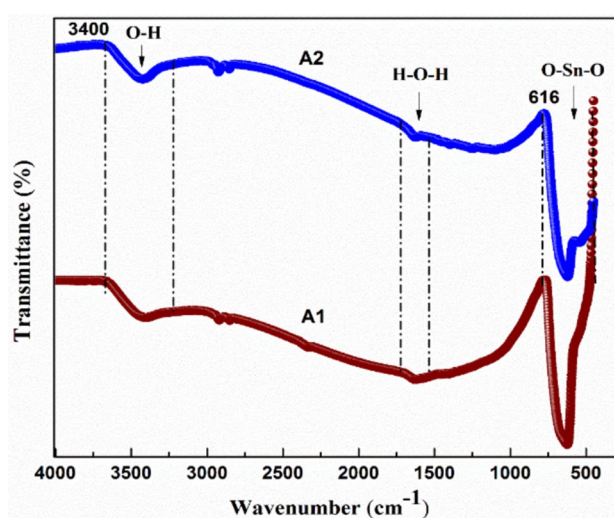Photoluminescence collectively provide insight into molecular, structural defects and impurities. Figure 4

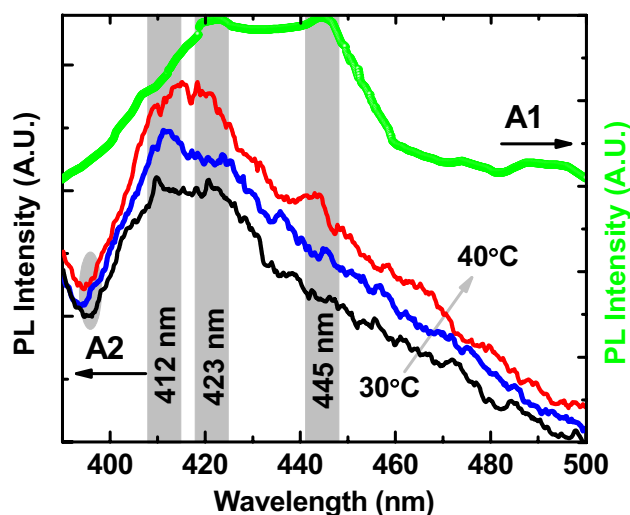**Fig. 3** FTIR spectra of (A1) pure SnO_2 and (A2) Schiff base-doped SnO_2

Fig. 4 PL spectra of (A1) pure SnO_2 and (A2) Schiff base-doped SnO_2

shows photoluminescence (PL) emission spectra of pure and doped SnO_2 specimen in the wavelength region of 390 nm to 500 nm. PL spectra of pure SnO_2 exhibits two prominent anomalies at ~ 423 nm and 445 nm [24]. Since the maxima of this emission spectra ~ 423 nm (2.93 eV) and 445 nm (2.78 eV) is far below from band gap, 3.62 eV (344 nm) of SnO_2. This infers that observed prominent peaks in PL spectra are not inherently associated with recombination activity between a conduction electron in the Sn 4p band and a hole in the O 2p valence band [25–28]. Further, these PL activities may be devoted to some indirect luminescent active centers. These indirect radiative centers introduce intermediate energy levels caused by defects such as interstitial defects, cation/anion vacancies, and dangling bonds. In transition metal oxides, the anionic vacancies V_O^0, V_O^+, and V_O^{++} act as main radiative center and traps conduction electrons. The V_O^{++} vacancies play active role in the visible range which indicated that V_O^{++} vacancy is governing the physical activity in SnO_2 and doped SnO_2. Former two anomalies are also visible in Schiff-based SnO_2 (A2) and we observe additional peak at 412 nm. To explore origin of the peak at 412 nm, temperature dependence of PL spectra for doped material has been studied. On the elevation of temperature, peak become more noticeable and shows a redshift characteristic. Thus, optical activity reported in the wavelength range of 400–500 nm suggests that nanoparticles of A1 and A2 possess anionic vacancies [29]. This peak nature may be attributed to thermally induced metastable defects energy levels. The fragile nature of the peak suggests that Schiff base doping may open another route to modulate edges of conduction band and to achieve desired optical properties. Schematic energy diagram of pure SnO_2 and Schiff-based SnO_2 derived from PL emission spectra is illustrated in Fig. 5. The anionic vacancies are known

to be responsible for various functionality in transition metal oxides. Here, we explore resistive switching property of synthesized samples.

Current voltage characteristics curves were recorded at room temperature using two probe technique, both source and sensing with same terminal. The switching reproducibility of I-V characteristics over 100 cycle is observed. Switching behavior observed in SnO_2 was found to be free of fluctuation. During the ascending branch of I-V measurements, the switching voltage was 12.5 V. Further, reversal branch of I-V characteristics suggests switching voltage is 9 V. In principle, on the basis of I-V profile the resistive switching phenomenon may be classified in two major classes; digital and analogue switching. The analogues switching exhibits gradual (non-monotonic) change in with applied electric field. I-V characteristics of SnO_2 were found to exhibit step like switching. Step like switching corresponds to digital switching On (1) – OFF (0) state. In ON state, SnO_2 exhibits lower resistive state that is called low resistive state (LRS), while in OFF state, the material exhibits higher resistive state (HRS). As the concept of switching refers that steep change in parameters (resistivity) along with the variation of its conjugate parameters. From technological point of view, steep switching in desired parameters are highly desirable especially for the memory and storage purpose.

A steep change in electrical conduction in metal oxides is devoted to the active role of Ag^+ ions of electrode and constituent ion oxygen as O^{2-} which suggests that the formation of Ag^+ filament is more dynamic than the other electrode metals [30]. Field driven rearrangement of Ag^+ and O^{2-} forms conducting filament, provides less resistive path to the current carriers. Most reliable theory toward the hysteretic nature of I-V curve is based on formation

Fig. 5 Schematic energy diagram of (A1) pure SnO_2 and (A2) Schiff base-doped SnO_2
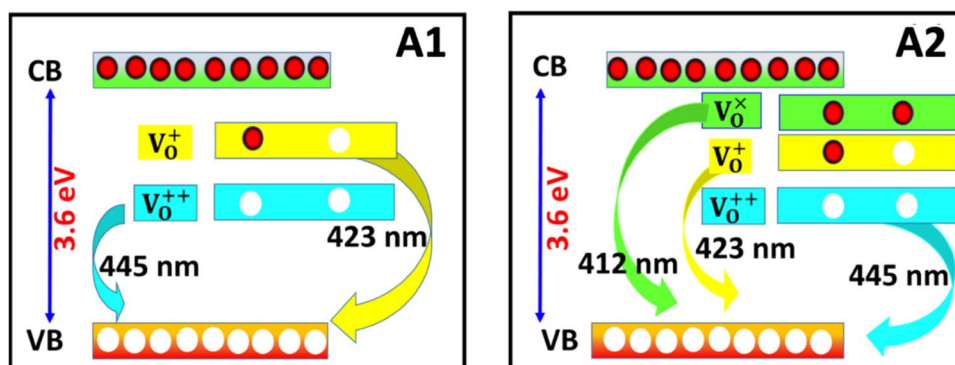
of conducting filament of mobile ions (electrode metal and oxygen anions). This filament mechanism involves role of different conducting path. The conducting filament is formed in presence of electric field; metal oxide changes its state from HRS to LRS. When mature conducting filament is exposed to the electric field of reversed polarity, the topology of filament is modified and conduction phenomenon is suppressed. Further, defects/vacancies are believed to be origin of conductivity in SnO_2 [31]. The suppression of electrical conductivity suggests that breaking of conducting filament has occurred. In SnO_2, we get hysteresis in I-V characteristics which is different from the non-volatile resistive switching and are shown in Fig. 6. Here, we observed a transition from LRS to HRS at E > 0. Switching from LRS to HRS without reversal of electric field signals that filamentary formation/disruption is not playing vital role. Here, we propose a barrier formation via charge trapping/detrapping process.

S. Almieda et al. has investigated thin film of SnO_2 on glass substrate, deposited by RF magnetron reactive sputtering at room temperature [32]. SnO_2 was characterized in form of $Ag/SnO_2/Ti$ structures. In this study, they realized the filamentary type mechanism via varying the area of electrical contacts. High field conduction process in this configuration was not of Ohmic type. They also do not find its compatibility with other conduction mechanism such as Poole-Frankel, Schottky emission or space-charge-limited conduction. Switching phenomenon of SnO_2 was finally attributed to change in structure.

Defects in nanoparticles of SnO_2 causes various physical properties which remain unavailable in its bulk form. To explore nature of oxygen vacancies and vacancy driven magnetism, isothermal magnetization vs external magnetic field has been performed, as shown in Fig. 7. Magnetization (M) is found to be
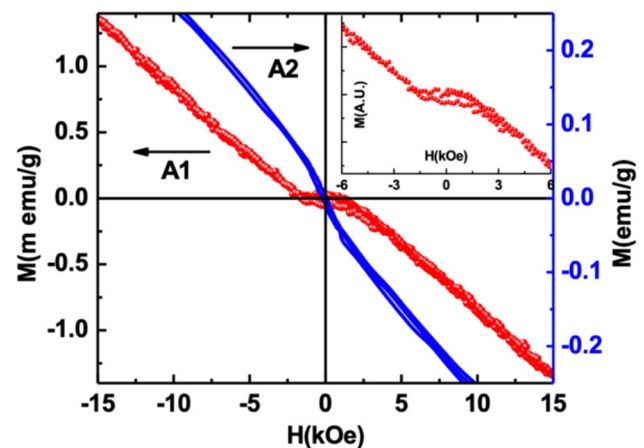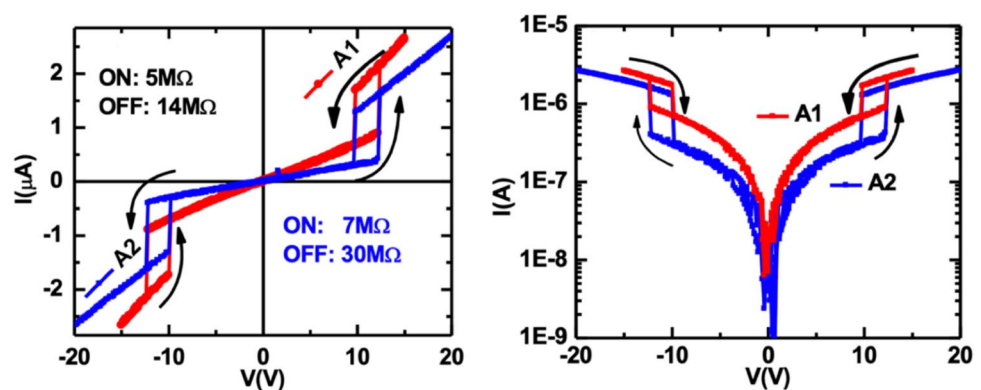

Fig. 7 M-H plots for (A1) pure SnO_2 and (A2) Schiff base-doped SnO_2

increasing in negative direction with increasing magnetic field (H) which shows diamagnetic behavior of both synthesized A1 and A2. In low field region ($-1.5kOe < H + 1.5kOe$), M vs H curve of specimen A1 shows hysteretic nature (shown in inset of Fig. 7 which signifies weak ferromagnetic characteristics of A1. Specimen A2 exhibits linear response in M(H) curve. Specimen A2 changes rate of magnetization for $H > 1.5kOe$ which further indicates about paramagnetic nature. To visualize this effect, we examined derivative dM/dH as function of external field H as shown in Fig. 8. Obtained derivative remains negative for both samples.

The dM/dH curve for A1 varies slowly while derivative is steeper for A2. This disappearance of hysteresis is consistent PL spectra and may be attributed to significant contribution of $V_O^\times$ and consistent with PL spectra. As in metal oxides, oxygen vacancies may be attained distinct charge, magnetic state, wavelength specific visible luminescence and

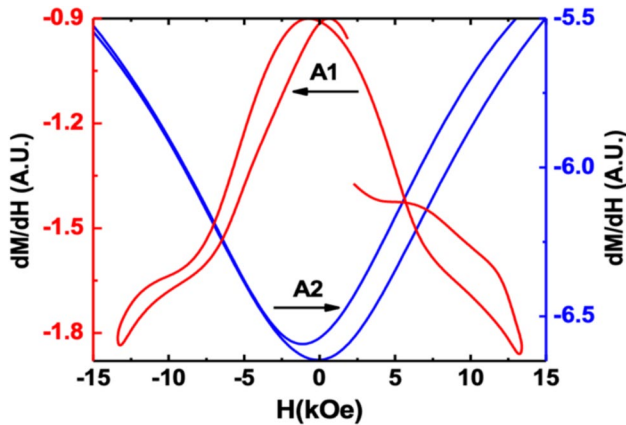**Fig. 6** IV characteristics of (A1) pure SnO_2 and (A2) Schiff base-doped SnO_2

Fig. 8 dM/dH curves for (A1) pure SnO_2 and (A2) Schiff base-doped SnO_2

recombination center due to having intermediate energy, $E_{VO,}$ ($E_{VB} < E_{VO} < E_{CB}$) [33]. The oxygen vacancy V_O^+ exhibits one unpaired electron which will contribute as paramagnetic identity. $V_O^\times$ exhibits pair of delocalized electrons and corresponding energy levels lies close to the conduction band due to correlation energy of two electrons. $V_O^\times$ is fragile in nature against the thermal activity and in ambient condition $V_O^\times$ remain optically inactive in pure SnO_2 due to thermal conversion of $V_O^\times$ into V_O^+ and e_{CB}' while Schiff base-modified SnO_2 exhibits peaks corresponding to $V_O^\times$ at 412 eV.

4 Conclusion

In summary, we characterized nano-sized SnO_2 and Schiff-based SnO_2 using XRD, TEM, FTIR, PL spectra, I-V characteristics, and isothermal magnetization. Diffraction studies reveal that particles size of synthesized SnO_2 and Schiff-based SnO_2 is of order of ~ 20 nm. Conventional characteristic peaks appeared in PL spectra are observed in SnO_2 and Schiff-based SnO_2 exhibits additional PL peak centered at 412 nm. This additional peak corresponds to $V_O^\times$ which remain absent in PL spectra of SnO_2 and ZnO type materials. It may be inferred that Schiff base modulation can be employed to enrich PL spectra for various technological application. Further, resistive switching characteristics of SnO_2 and Schiff base SnO_2 has been investigated. This study reveals that Schiff base doping offers robust resistive switching property.

Author contributions

Monika Duhan: Conceptualization, Methodology, Investigation, Writing—Original Draft. Manpreet Kaur: Data Curation, Methodology, Investigation, Writing. Sanjeev Kumar: Investigation, Visualization, Writing—Review & Editing. Gyaneshwar Sharma: Conceptualization, Methodology, Investigation, Review. Harminder Kaur: Conceptualization, Supervision, Funding Acquisition, Review & Editing.

Data availability

Data available upon request: The data that support the findings of this study are available from the corresponding author upon request.

Declarations

Conflict of interest The authors declare no conflict of interest.

References

1. D.S. Jeong, R. Thomas, R.S. Katiyar, J.F. Scott, H. Kohlstedt, A. Petraru, C.S. Hwang, Emerging memories: resistive switching mechanisms and current status. Rep. Prog. Phys. **75**(7), 076502 (2012). https://doi.org/10.1088/0034-4885/75/7/076502

2. R. Waser, M. Aono, Nanoionics-based resistive switching memories. Nanosci. Technol. (2009). https://doi.org/10.1142/9789814287005_0016

3. D.B. Strukov, G.S. Snider, D.R. Stewart, R.S. Williams, The missing memristor found. Nature **453**(7191), 80–83 (2008). https://doi.org/10.1038/nature06932

4. S. Seo, M.J. Lee, D.H. Seo, E.J. Jeoung, D.-S. Suh, Y.S. Joung, B.H. Park, Reproducible resistance switching in

polycrystalline NiO films. Appl. Phys. Lett. **85**(23), 5655–5657 (2004). https://doi.org/10.1063/1.1831560

5. G.I. Meijer, Materials science: who wins the nonvolatile memory race? Science **319**(5870), 1625–1626 (2008). https://doi.org/10.1126/science.1153909

6. A. Kalateh, A. Jalali, M.J. Kamali Ashtiani et al., Resistive switching transparent SnO2 thin film sensitive to light and humidity. Sci. Rep. **13**, 20036 (2023). https://doi.org/10.1038/s41598-023-45790-0

7. M. Akbari-Saatlu, M. Schalk, S. Pokhrel, C. Mattsson, L. Mädler, M. Procek, Ultrasensitive H$_2$S and CH$_3$SH sensors based on SnO$_2$ porous structures utilizing combination of flame and ultrasonic spray pyrolysis methods. IEEE Sens. J. **24**(22), 36393–36402 (2024). https://doi.org/10.1109/JSEN.2024.3467168

8. S. Koliopoulou, P. Dimitrakis, D. Goustouridis, P. Normand, C. Pearson, M.C. Petty, H. Radamson, D. Tsoukalas, Metal nano-floating gate memory devices fabricated at low temperature. Microelectron. Eng. **83**, 1563–1566 (2006). https://doi.org/10.1016/j.mee.2006.01.235

9. S. Kim, Y.-K. Choi, A comprehensive study of the resistive switching mechanism in Al/TiO$_x$TiO$_{2-x}$Al-structured RRAM. IEEE Trans. Electron Devices **56**(12), 3049–3054 (2009). https://doi.org/10.1109/ted.2009.2032597

10. H.-S.P. Wong, H.-Y. Lee, S. Yu, Y.-S. Chen, Y. Wu, P.-S. Chen, M.-J. Tsai, Metal-Oxide RRAM. Proc. IEEE **100**(6), 1951–1970 (2012). https://doi.org/10.1109/jproc.2012.2190369

11. H.Y. Lee, P.S. Chen, T.Y. Wu, Y.S. Chen, C.C. Wang, P.J. Tzeng, M.J. Tsai, Low power and high speed bipolar switching with a thin reactive Ti buffer layer in robust HfO2 based RRAM. 2008 IEEE International Electron Devices Meeting (2008). https://doi.org/10.1109/iedm.2008.4796677

12. X. Cao, X. Li, X. Gao, X. Liu, C. Yang, R. Yang, P. Jin, All-ZnO-based transparent resistance random access memory device fully fabricated at room temperature. J. Phys. D Appl. Phys. **44**(25), 255104 (2011). https://doi.org/10.1088/0022-3727/44/25/255104

13. Y. Wu, B. Lee, H.-S.P. Wong, $\hbox{Al}_{2}\hbox{O}_{3}$-based RRAM using atomic layer deposition (ALD) With 1-$\mu\hbox{A}$ RESET current. IEEE Electron Device Lett. **31**(12), 1449–1451 (2010). https://doi.org/10.1109/led.2010.2074177

14. S.K. Pradhan, B. Xiao, S. Mishra, A. Killam, A.K. Pradhan, Resistive switching behavior of reduced graphene oxide memory cells for low power nonvolatile device application. Sci. Rep. (2016). https://doi.org/10.1038/srep26763

15. Yu. Lee-Eun, S. Kim, M.-K. Ryu, S.-Y. Choi, Y.-K. Choi, Structure effects on resistive switching of $\hbox{Al/TiO}_{x}/\hbox{Al}$ devices for RRAM applications. IEEE Electron Device Lett. **29**(4), 331–333 (2008). https://doi.org/10.1109/led.2008.918253

16. C.-C. Lin, C.-Y. Lin, M.-H. Lin, C.-H. Lin, T.-Y. Tseng, Voltage-polarity-independent and high-speed resistive switching properties of V-doped $\hbox{SrZrO}_{3}$ thin films. IEEE Trans. Electron Devices **54**(12), 3146–3151 (2007). https://doi.org/10.1109/ted.2007.908867

17. K. Nagashima, T. Yanagida, K. Oka, T. Kawai, Unipolar resistive switching characteristics of room temperature grown SnO2 thin films. Appl. Phys. Lett. **94**(24), 242902 (2009). https://doi.org/10.1063/1.3156863

18. M. Naseh, T. Sedaghat, A. Tarassoli, E. Shakerzadeh, DFT studies of ONO Schiff bases, their anions and diorganotin(IV) complexes: tautomerism NBO and AIM analysis. Comput. Theor. Chem. **1005**, 53–57 (2013). https://doi.org/10.1016/j.comptc.2012.11.004

19. M.C. García-López, B.M. Muñoz-Flores, V.M. Jiménez-Pérez, I. Moggio, E. Arias, R. Chan-Navarro, R. Santillan, Synthesis and photophysical characterization of organotin compounds derived from Schiff bases for organic light emitting diodes. Dyes Pigm. **106**, 188–196 (2014). https://doi.org/10.1016/j.dyepig.2014.02.021

20. M. Duhan, H. Kaur, R. Bhardwaj, N. Kumar, S. Kumar, A. Gupta, S. Gautam, Magnetic metamorphosis of structurally enriched sol-gel derived SnO2 nanoparticles. Vacuum (2018). https://doi.org/10.1016/j.vacuum.2018.11.025

21. K. Prakash, P. Senthil Kumar, S. Pandiaraj, K. Saravanakumar, S. Karuthapandian, Controllable synthesis of SnO-2photocatalyst with superior photocatalytic activity for the degradation of methylene blue dye solution. J. Exp. Nanosci. **11**(14), 1138–1155 (2016). https://doi.org/10.1080/17458080.2016.1188222

22. F.A. Akgul, C. Gumus, A.O. Er, A.H. Farha, G. Akgul, Y. Ufuktepe, Z. Liu, Structural and electronic properties of SnO$_2$. J. Alloy. Compd. **579**, 50–56 (2013). https://doi.org/10.1016/j.jallcom.2013.05.057

23. L. Jiang, G. Sun, Z. Zhou, S. Sun, Q. Wang, S. Yan, Q. Xin, Size-controllable synthesis of monodispersed SnO$_2$ nanoparticles and application in electrocatalysts. J. Phys. Chem. B **109**(18), 8774–8778 (2005). https://doi.org/10.1021/jp050334g

24. S.G. Ghugal, S.S. Umare, R. Sasikala, A stable, efficient and reusable CdS–SnO2 heterostructured photocatalyst for the mineralization of Acid Violet 7 dye. Appl. Catal. A **496**, 25–31 (2015). https://doi.org/10.1016/j.apcata.2015.02.035

25. R.K. Mishra, A. Kushwaha, P.P. Sahay, Influence of Cu doping on the structural, photoluminescence and formaldehyde sensing properties of SnO2nanoparticles. RSC Adv.

4(8), 3904–3912 (2014). https://doi.org/10.1039/c3ra43709d

26. P.S. Chowdhury, S. Saha, A. Patra, Influence of nanoenvironment on luminescence of Eu3+activated SnO_2 nanocrystals. Solid State Commun. **131**(12), 785–788 (2004). https://doi.org/10.1016/j.ssc.2004.06.040

27. A. Kar, A. Patra, Optical and electrical properties of Eu3+-doped SnO_2 nanocrystals. J. Phys. Chem. C **113**(11), 4375–4380 (2009). https://doi.org/10.1021/jp810777f

28. E.J.H. Lee, C. Ribeiro, T.R. Giraldi, E. Longo, E.R. Leite, J.A. Varela, Photoluminescence in quantum-confined SnO2 nanocrystals: evidence of free exciton decay. Appl. Phys. Lett. **84**(10), 1745–1747 (2004). https://doi.org/10.1063/1.1655693

29. F. Gu, S.F. Wang, M.K. Lü, X.F. Cheng, S.W. Liu, G.J. Zhou, D.R. Yuan, Luminescence of SnO2 thin films prepared by spin-coating method. J. Cryst. Growth **262**(1–4), 182–185 (2004). https://doi.org/10.1016/j.jcrysgro.2003.10.028

30. T. Wan, B. Qu, H. Du, X. Lin, Q. Lin, D.-W. Wang, D. Chu, Digital to analog resistive switching transition induced by graphene buffer layer in strontium titanate based devices. J. Colloid Interface Sci. **512**, 767–774 (2018). https://doi.org/10.1016/j.jcis.2017.10.113

31. F.E. Ghodsi, J. Mazloom, Optical, electrical and morphological properties of p-type Mn-doped SnO2 nanostructured thin films prepared by sol–gel process. Appl. Phys. A **108**(3), 693–700 (2012). https://doi.org/10.1007/s00339-012-6952-0

32. S. Almeida, B. Aguirre, N. Marquez, J. McClure, D. Zubia, Resistive switching of SnO2 thin films on glass substrates. Integr. Ferroelectr. **126**(1), 117–124 (2011). https://doi.org/10.1080/10584587.2011.575015

33. F. Gu, S.F. Wang, M.K. Lü, G.J. Zhou, D. Xu, D.R. Yuan, Photoluminescence properties of SnO_2 nanoparticles synthesized by Sol−Gel method. J. Phys. Chem. B **108**(24), 8119–8123 (2004). https://doi.org/10.1021/jp036741e